The OH-Initiated Oxidation of 1,3-Butadiene in the Presence of O_2 and NO: A Photolytic Route To Study Isomeric Selective Reactivity

Erin E. Greenwald,[†] Jiho Park,[†] Katie C. Anderson,[†] Hahkjoon Kim,[†] B. Jesse E. Reich,[†] Stephen A. Miller,[†] Renyi Zhang,[‡] and Simon W. North*,[†]

Department of Chemistry, Texas A&M University, P.O. Box 30012, College Station, Texas 77842, and Department of Atmospheric Sciences, Texas A&M University, College Station, Texas 77842

Received: March 25, 2005; In Final Form: June 27, 2005

We report the study of the isomeric selective OH-initiated oxidation of 1,3-butadiene in the presence of O_2 and NO using the LP/LIF technique. The photolysis of monodeuterated 1-iodo-3-buten-2-ol provides only one of the possible OD-butadiene adducts, the minor addition channel product, simplifying the oxidation mechanism. We find, based on analysis of OD time-dependent traces that prompt rearrangement of initial β-hydroxyalkyl radicals to α-hydroxyalkyl radicals occurs in agreement with RRKM/ME theoretical predictions. We report a rate constant of $(3.3\pm1.0) \times 10^{-11}$ cm^3 molecules^{-1} s^{-1} for deuterium abstraction from the α-hydroxyalkyl radical at 298 $\pm$2 K. Our approach demonstrates the feasibility of isomeric selective kinetic studies of the OH-initiated oxidation of unsaturated hydrocarbons.

I. Introduction

There is considerable interest in the atmospheric oxidation of unsaturated hydrocarbons due to their role in ozone production, aerosol formation, and acid rain.[1] Although significant progress has been made toward unraveling the detailed mechanisms of OH-initiated oxidation, questions persist. In the case of larger unsaturated hydrocarbons, like isoprene, the electrophilic addition of OH results in multiple radical isomers. Often the number of intermediate species increases following the reaction with O_2 and further branching can occur during subsequent steps on the way to first generation end products. Although recent ab initio studies[2−9] have made a substantial impact in providing a priori predictions of these branching ratios in isoprene oxidation, direct experimental confirmation is unavailable. Recent kinetic studies have relied on OH regeneration to infer information about the isomeric branching.[10−14] Analysis of the results suggests qualitative agreement with theoretical predictions but the complexity of the reaction systems has precluded a quantitative comparison. To date all of the kinetic data reflect "lumped", nonisomeric selective, rate constants. Direct measurements of the intermediates using either chemical ionization mass spectrometry[15] or transient absorption have also been unable to extract isomeric specific rate constants and branching ratios. Zalyubovsky and co-workers have recently demonstrated the feasibility of using cavity ring-down spectroscopy on the resolved A−X transition of peroxy radicals to obtain selective detection.[16] In those studies, the peroxy radicals were generated via reaction of a hydrocarbon with OH in the presence of O_2. As the hydrocarbons become more complex and the resulting number of isomers increases, however, the spectroscopic assignments will be challenging. Ideally one would like to isolate the isomers and thus simplify the ensuing kinetics. In addition to making kinetic studies more tractable, isomeric selective studies permit the investigation of minor, yet important, channels that are difficult to study in the presence of major channel kinetics. The photodissociation of a suitable precursor can, in principle, provide a route to the formation of a single isomer.

In the present study, we focus on the photolytic production of one of two possible isomers following OH reaction with 1,3-butadiene, the addition of OH to the inner carbons, to demonstrate the feasibility of this approach. It is expected that this is the minor channel, based on the analogous methyl-substituted butadiene (2-methyl-1,3-butadiene)[2−4,17−20] where there is preferential addition of OH to one of the terminal carbons. There are several requirements which must be considered prior to selecting a photolytic precursor. The photodissociation should have an appreciable absorption cross-section at the photolysis wavelength and result in a single product channel with near unity quantum yield. There is an additional, more subtle, requirement, which is particularly relevant in the present study. The thermal addition of OH to 1,3-butadiene results in a highly activated radical with internal energy in excess of the exothermicity of the reaction. Thus, to mimic subsequent reactivity of these radicals under thermal conditions, the photolytic route must result in a nascent energy distribution consistent with thermal activation. Halogenated compounds are suitable precursors since excitation in the UV/vis region typically involves an n $\rightarrow \sigma^*$ transition on the C−X moiety resulting in prompt dissociation of this bond. Given the relative bond strengths of the carbon−halogen bonds, the location of the corresponding absorption maxima in the UV/vis region, and the energy partitioning predicted for a direct dissociation on a repulsive potential,[21] we find that the iodine-substituted compounds are ideal. To this end, we have synthesized the photolytic precursor, 1-iodo-3-buten-2-ol (**1**). Photolysis at 266 nm should produce activated β-hydroxyalkyl radical **2a**, one of the two possible adducts following OH addition to 1,3-butadiene. We are particularly interested in this radical due to the cyclic rearrangement pathway, which leads to an α-hydroxyalkyl radical. Although this isomerization pathway, 3-exo-trig, is well-known in solution,[22] to our knowledge, the first discussion of this chemistry

* Address correspondence to this author.
[†] Department of Chemistry.
[‡] Department of Atmospheric Sciences.

10.1021/jp051545o CCC: $30.25
Published on Web 08/13/2005

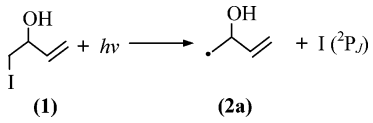

(1) **(2a)**

in the gas phase appeared in the context of isoprene oxidation, as the result of addition of OH to conjugated, unsaturated hydrocarbons.[23] The reaction of α-hydroxyalkyl radicals with O_2 proceeds via hydrogen abstraction, resulting in carbonyls and HO_2, whereas the dominant fate of β-hydroxyalkyl radicals in the presence of O_2 is addition to yield peroxy radicals.[24−27]

The present paper coalesces the results of several computational and experimental studies, each of which plays a vital role in demonstrating the viability of this approach. Velocity map ion imaging (VELMI) experiments are used to determine the nascent energy distribution of the β-hydroxyalkyl radicals (Section IIIA). The energetics of the isomerization reaction are evaluated using quantum chemical calculations, and the final branching ratios between the β-hydroxyalkyl and α-hydroxyalkyl radicals are determined using RRKM theory coupled with the master equation formalism (Section IIIB). Finally, the kinetics of the OD formation in the presence of O_2 and NO has been studied using the LP/LIF technique. The results confirm a significant yield of α-hydroxyalkyl radicals and provide a 298 ± 2 K rate constant for the α-hydroxyalkyl radical reaction with O_2 (Section IIIC). This proof-of-principle study demonstrates the feasibility of isomeric selective kinetic studies of the OH-initiated oxidation of unsaturated hydrocarbons.

II. Experimental Section

The synthesis of 1-iodo-3-buten-2-ol was based on an approach to iodohydrins reported of Ishii et al.[28] Identification and purity of the sample was confirmed by comparison of NMR spectra with the report of Masuda et al.[29] Monodeuteration of the sample was achieved by shaking 1-iodo-3-buten-2-ol in an ether/D_2O mixture.

The photodissociation dynamics of 1-iodo-3-buten-2-ol at 266 nm were studied using velocity-map imaging.[30] Details of the apparatus will be presented elsewhere.[31] Briefly, a pulsed molecular beam of 1% 1-iodo-3-butene-2-ol in He (1 atm) was collimated by a conical skimmer and crossed at 90° by the focused output of a tunable pulsed laser beam. A single color near 266 nm was used for both photolysis and state-selective ionization of the iodine atom photofragments using 2+1 resonance-enhanced multiphoton ionization (REMPI).[32] The light near 266 nm was generated by doubling the output of an Nd:YAG (Spectra-Physics LAB-150-10) pumped dye laser (LAS). The resulting ions were accelerated the length of a 50 cm flight tube and detected by a 40 mm diameter dual microchannel plate (MCP) coupled to a phosphor screen assembly. The MCP plates were gated to collect only *m*/*z* 127. Images were collected with a fast scan charge-coupled device camera and integrated using a data acquisition system. A PMT assembly was used to measure ion arrival times in order to select the timing gate of the MCP.

The detailed description of the laser photolysis/laser-induced fluorescence (LP/LIF) experiments has been reported elsewhere[3,12] and only the essential features are described. The kinetics experiments were performed on the monodeuterated sample and OD was probed to eliminate ambiguous assignment of the origin of OH formation. However, experiments employing 1-iodo-3-buten-2-ol or monodeuterated 1-iodo-3-buten-2-ol, and probing either OH or OD formation, respectively, exhibited almost identical time-dependent behavior at early times (i.e., in the first 80 μs). The unfocused 266 nm beam from an Nd:YAG laser (Spectra Physics GCR-150-10) was used to photolyze 1-iodo-3-buten-2-ol. The LIF technique was used to monitor OH or OD excited on the $Q_1(1)$ transition of the A←X(1,0) vibrational band near 282 or 287 nm, respectively, using the BBO-doubled output of a pulsed dye laser (Quantel TDL-51) running Rhodamine 590 pumped at 532 nm by an Nd:YAG laser (Spectra Physics GCR-150-10). Each fluorescence decay was averaged over multiple shots and integrated. The repetition rate of the lasers was set at 10 Hz and the delay between photolysis and probe lasers was controlled by a digital delay/pulse generator (SRS, DG-535). The 1-iodo-3-buten-2-ol was introduced into the cell as a mixture with argon. Both the NO (Aldrich, 98.5%) and the O_2 (BOTCo, 99.6%) were buffered with argon in 5-L bulbs to known concentrations and were introduced into the cell through flow meters. The NO was purified to remove HONO and NO_2 impurities by passing it through an ascarite trap prior to mixing with argon. The concentration of NO in the reaction cell was varied from 2.99×10^{14} to 1.30×10^{15} molecules cm^{-3} and the concentration of O_2 in the reaction cell was varied from 4.20×10^{14} to 1.69×10^{15} molecules cm^{-3}. Several experiments were run with fixed concentrations of 1-iodo-3-buten-2-ol at room temperature (298 ± 2 K) while the concentration of NO or O_2 was varied. The total pressure in the cell was maintained at 50 Torr by buffering with argon.

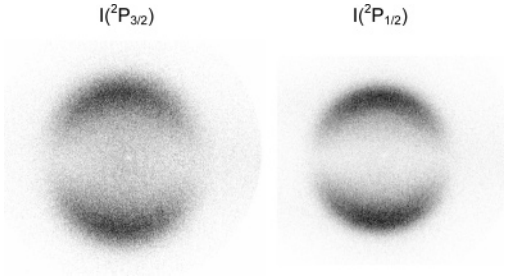

Figure 1. Raw ion images for I($^2P_{3/2}$) (left) and I($^2P_{1/2}$) (right) atoms from the photodissociation of 1-iodo-2-butene-3-ol at 266 nm.

III. Results and Discussion

A. Ion Imaging Experiments. Raw photofragment images for I($^2P_{3/2}$) and I($^2P_{1/2}$) (hereafter referred to as I and I*, respectively) are shown in Figure 1. The electric field vector of the laser is vertical in the plane of the image. The images represent 2D projections of the 3D velocity distributions. Conversion of the raw images into speed and angular distributions was achieved using the basis set expansion program (BASEX) for image reconstruction developed by Reisler and co-workers.[33] The photofragment angular distributions can be described by the form[34]

$$P(\theta) \propto \frac{1}{4\pi}[1 + \beta P_2(\cos\theta)]$$

where β is the spatial anisotropy parameter and $P_2(\cos\theta)$ is the second Legendre polynomial. We have determined a best fit speed-independent anisotropy parameter of $\beta = 1.4 \pm 0.1$ for both channels, consistent with a parallel transition to a repulsive excited-state potential.

The I/I* branching ratio was determined by integration of the Doppler profiles for the I/I* transitions using identical laser power. The integrated Doppler profiles were weighted by the relative detection efficiencies of I and I* at 266 nm.[35] Independent confirmation of the detection efficiencies was

TABLE 1: Relative Energies (in kcal/mol), Including Spin−Orbit Splitting for the OH and Zero Point Energy, for the Isomers at Various Levels of Theory

method and basis set[a]	C_4H_6 + OH	2a	ts1	2b	ts2	2c
B3LYP/6-31G*	22.4	0.0	9.7	3.0	8.6	−6.1
B3LYP/6-311++G**	18.9	0.0	10.1	4.5	8.9	−6.3
CCSD(T)/cc-pVDZ//B3LYP/6-311++G**	23.4	0.0	12.7	5.1	12.8	−4.9
CCSD(T)/cc-pVTZ//B3LYP/6-311++G**	22.4	0.0	11.5	4.5	11.6	−4.9

[a] CCSD(T) calculations include zero point energy from the B3LYP/6-311++G** frequency calculation.

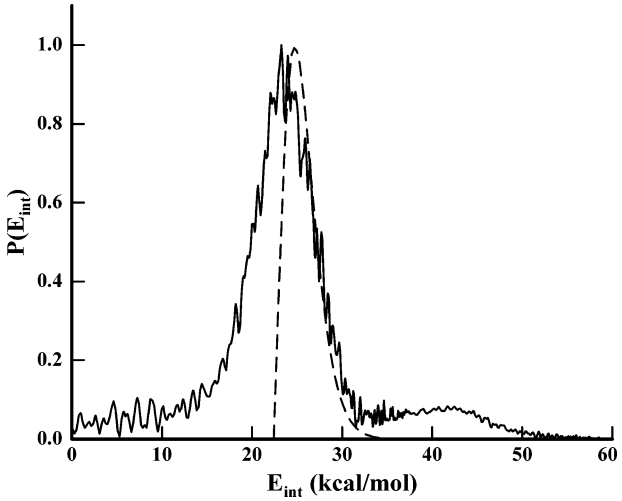

Figure 2. Nascent β-hydroxyalkyl radical internal energy distribution (solid line) based on the measured translational energy derived from the ion imaging data shown in Figure 1. The dashed line represents a shifted 300 K Boltzmann distribution.

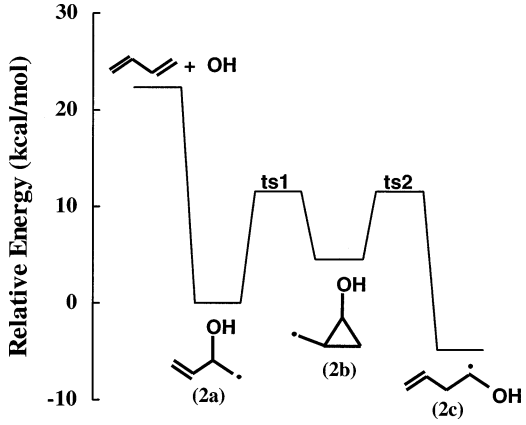

Figure 3. Schematic reaction diagram for the cyclic isomerization reaction of the OH-butadiene radical obtained using CCSD(T)/cc-pVTZ//B3LYP/6-311++G** energies (including B3LYP/6-311++G** zero point energy) and spin-orbit splitting for the OH.

obtained using the photodissociation of CH_3I at 266 nm. Based on this analysis, we have determined fractional yields for I and I* of 0.12 and 0.88, respectively. The energy partitioning and I/I* branching ratio are very similar to the results of previous alkyl iodide photolysis near 260 nm.[36,37,38]

The internal energy distribution of the nascent radicals formed in coincidence with either I or I* products can be obtained from the measured translational energy distributions of I and I* using energy conservation

$$E_{\text{avail}} = h\nu - D_0^0(\text{C}-\text{I}) = E_{\text{trans}} + E_{\text{SO}}(\text{I}) + E_{\text{R,V}}(C_4H_6OH)$$

where D^0_0(C−I) is the C−I bond dissociation energy, calculated at the B3LYP/6-311G** level of theory to be 47.7 kcal/mol,[39] E_{SO}(I) is the iodine spin−orbit energy, and $E_{\text{R,V}}(C_4H_6OH)$ is the rovibrational energy content of the β-hydroxyalkyl radical. The final energy distribution is shown as the solid line in Figure 2. For comparison a 300 K Boltzmann energy distribution, shifted by the exothermicity of the addition of OH to the inner position of 1,3-butadiene, as would be predicted for chemical activation, is shown as the dashed line in Figure 2. The distributions are qualitatively similar suggesting that the subsequent kinetics of the radicals produced via photolysis of 1-iodo-3-buten-2-ol should effectively mimic the radicals formed by thermal recombination.[40] The measured internal energy distribution is bimodal as a result of the large spin−orbit splitting between the two atomic states of iodine. The small peak, centered around 40 kcal/mol, corresponds to the ground state I; whereas, the large peak centered around 22 kcal/mol corresponds to I*. The relative heights of these peaks reflect the I/I* branching ratio. Since the I/I* branching ratio will be dependent on the dissociation wavelength and a change to this ratio can significantly alter the nascent energy distribution, careful measurements of the I/I* ratio must be performed to assess this affect. Increasing the dissociation wavelength could, in fact, result in an internal energy distribution of nascent hydroxyalkyl radicals which is hotter than that at 266 nm if the I/I* branching ratio increased.

B. Calculations of the Cyclic Isomerization Reactions. Quantum chemical calculations using the Gaussian 03[41] software package were performed to provide all relevant energetics, geometries, and frequencies to obtain state counts as a function of energy for the OH-butadiene adduct radical cyclic isomerization reaction. The highest level calculations performed, which were used in the kinetic modeling, include optimized geometries of reactants, intermediate species, products, and transition states using density functional theory (DFT). Becke's three-parameter hybrid method employing the LYP correlation functional (B3LYP)[42,43] in conjunction with the Pople-style triple-ζ split valence polarized basis sets was used (6-311++G**).[44,45] Single-point energy calculations were performed on these geometries using coupled-cluster theory with single and double excitations with perturbative inclusion of the triples contribution (CCSD(T))[46,47] with the Dunning-style triple-ζ basis sets (cc-pVTZ).[48] Energies from density functional theory and ab initio calculations are listed in Table 1 and a schematic energy diagram is shown in Figure 3.

The initially activated β-hydroxyalkyl radicals are subject to a competition between collisional stabilization, dissociation, and isomerization.[23] We have employed RRKM theory coupled with the master equation (ME) formalism to calculate reaction rate constants as well as branching ratios among the isomers and into the dissociative channel, to give 1,3-butadiene and OH. Since the OH-butadiene radicals isomerize through well-defined transition states along the potential energy surface, standard (nonvariational) RRKM theory can be used to calculate microcanonical rates. An accurate description of the dissociation of the OH-butadiene adduct requires a two transition state model, which includes variational treatments of both the inner and the outer transition states. Recently, this treatment has been applied

to the case of the hydroxyl radical addition to ethylene.[49] At high temperatures, the outer transition state becomes unimportant and the kinetic model can be accurately approximated by including only the flux through the inner transition state. At 300 K, the inner transition state serves as the dominant bottleneck such that an inclusion of both transition states only reduces the rate by 30%. Furthermore, high level ab initio calculations revealed that the potential energy surface for the adduct dissociation includes a saddle point below the asymptotic energy of separated products and the saddle point appears at carbon−oxygen separation distances of approximately 2.2 Å. For the purposes of this model, a 2.2 Å carbon−oxygen separation was assumed to adequately describe the saddle point for the adduct dissociation channel. A B3LYP/6-311++G** geometry optimization constraining the carbon−oxygen bond distance to 2.2 Å and frequency calculation were used to determine harmonic frequencies and rotational constants in order to evaluate the microcanonical number of states for the adduct dissociation channel. The threshold energy was assumed to be the asymptotic energy for separated 1,3-butadiene and OH. Neglecting variational effects introduces an error of less than 15% to the dissociation rate in the case of ethylene and has, therefore, been excluded from the current work.

CCSD(T)/cc-pVTZ//B3LYP/6-311++G** energies, unscaled vibrational frequencies, and rotational constants were used to calculate the RRKM rate constants through the transition states. For all species, the density and sum of states were obtained through an exact count procedure by the Stein−Rabinovitch extension[50] of the Beyer−Swinehart algorithm[51] implemented in the MultiWell program suite.[52,53] There was no reaction path degeneracy for the isomerization reactions. The dissociation channel for the OH-butadiene adduct was considered to be irreversible, and the isomerization steps were considered to be reversible. The transformation from the microcanonical rates to thermal rate constants and the short-time evolution of the initial OH-butadiene radical distribution were treated using the one-dimensional, energy-grained ME formalism. Implementation of the ME formalism includes activation and deactivation processes as well as unimolecular rate constants for reacting molecules.[52−54] The strong collision approximation is not valid for the treatment of small monatomic or diatomic colliders such as Ar or N_2. A more appropriate treatment includes a weak collision model, which has been implemented by applying the exponential down model of energy transfer. We have calculated collision frequencies based on a Lennard-Jones interaction potential. The necessary quantities for the self-collisions of many bath gases (e.g. Ar and N_2) and several reactant molecules are listed in the literature.[54] In the case of the hydroxyalkyl radicals, it is necessary to estimate ϵ and σ since these are not available. We calculated their values using empirical formulas.[54] The values of $\epsilon = 225.6$ and 146.4 K and $\sigma = 4.5$ and 4.8 Å have been adopted as Lennard-Jones parameters for the interactions between the hydroxyalkyl radicals with Ar and N_2, respectively. The average collisional energy transfer parameter ($\langle\Delta E_{down}\rangle$) was chosen to be 300 cm^{-1} as molecules of similar size have been shown to have experimentally determined collisional energy transfer parameters in the neighborhood of 300 cm^{-1}.[54] A change in the average collisional energy transfer ($\langle\Delta E_{down}\rangle$) by $\pm$100 cm^{-1} results in a change of less than $\pm$14% in the final steady-state population of 2**a** under the present laboratory conditions. Simulations using tropospheric conditions exhibit a change of $\pm$16%. Increasing $\langle\Delta E_{down}\rangle$, as with increasing the pressure or decreasing the temperature, results in a larger initial fraction of β-hydroxyalkyl radicals, reflecting more efficient collisional stabilization.

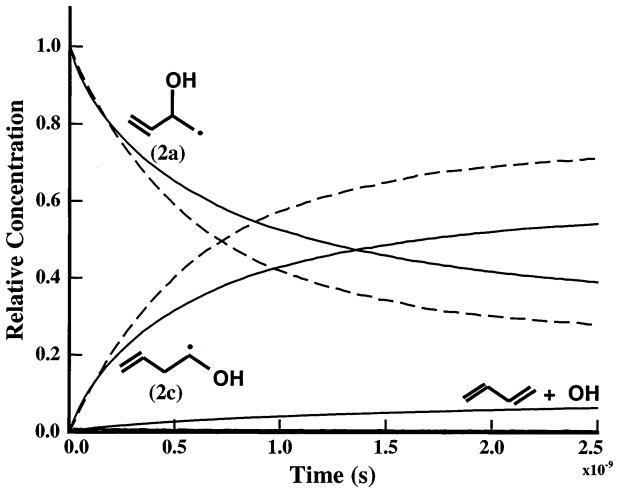

Figure 4. RRKM/ME modeling of the fractional populations of isomers as a function of time under laboratory conditions using the energy distribution shown in the solid line in Figure 2 as the β-hydroxyalkyl radical initial energy distribution (solid line); RRKM/ME modeling of the fractional populations of isomers as a function of time under laboratory conditions using a thermal distribution of energy, 298 K, as shown in the dashed line in Figure 2 (dashed line).

The present calculations focus on the prediction of the branching ratio between α- and β-hydroxyalkyl radicals to help explain the observed kinetic data shown in section IIIC. The measured internal energy distribution for the nascent β-hydroxyalkyl radicals from the photodissociation experiment was used as an initial energy distribution for a simulation at 50 Torr in an argon bath gas to model the chemistry in the laboratory experiments presented in section IIIC. RRKM/ME calculations were performed at 298 K and 760 Torr in a nitrogen atmosphere, applicable to tropospheric conditions, where a Boltzmann distribution, shifted by the exothermicity of the addition reaction, was used for the initial energy distribution of β-hydroxyalkyl radicals.[55] The fractional populations of the isomers as a function of time following photolytic preparation and under laboratory conditions are shown as the solid lines in Figure 4.

At 50 Torr total pressure in Ar and 298 K, the conditions of the present experiment, the fractional populations of isomers **2a**, **2b**, and **2c** reach quasi-steady-state values after 1×10^{-8} s, which can be considered prompt on the time scale of subsequent reaction with O_2. While the α-hydroxyalkyl radical is thermodynamically favored, the approach to equilibrium, which results in the quantitative conversion to the α-hydroxyalkyl radical, occurs at a significantly slower rate following initial collisional stabilization. At the smallest and largest O_2 concentrations used in the kinetics experiment, the lifetimes of the β-hydroxyalkyl radical in the presence of O_2 are 1 ms and 300 μs, which is faster than the approach to equilibrium.

In the troposphere, the fractional populations of isomers **2a**, **2b**, and **2c** reach quasi-steady-state values faster than 1×10^{-8} s, which can also be considered prompt on the time scale of subsequent reactivity. The lifetime of β-hydroxyalkyl radicals in the troposphere is less than 1 μs. The ratio of β-hydroxyalkyl radicals to α-hydroxyalkyl radicals in the troposphere is essentially determined by the initial collisional stabilization, where the majority of the population (0.64) is already in the α-hydroxyalkyl radical form. Since the fractional populations of α-hydroxyalkyl radicals and β-hydroxyalkyl radicals do not change significantly both in the temperature range from 240 to 340 K at 760 Torr and in the pressure range from 50 to 760

TABLE 2: Quasi-Steady-State Fractional Populations as a Function of Conditions[a]

	populations at the following conditions: temp/K; pressure/Torr; $\langle \Delta E_{down} \rangle$						
	*h*ν; 50;[b] 300	298; 50;[b] 300	298; 760;[c] 200	298; 760;[c] 300	298; 760;[c] 400	240; 760;[c] 300	340; 760;[c] 300
C_4H_6 + OH	0.11	0.02	<0.01	<0.01	<0.01	<0.01	<0.01
2a	0.22	0.15	0.26	0.36	0.46	0.48	0.30
2b	<0.01	<0.01	<0.01	<0.01	<0.01	<0.01	<0.01
2c	0.67	0.83	0.74	0.64	0.54	0.52	0.69

[a] All temperatures are modeled by the shifted Boltzmann except for *h*ν, which is the internal energy distribution measured by VELMI. [b] Argon bath gas and populations taken at $t = 1 \times 10^{-7}$ s. [c] N_2 bath gas and populations taken at $t = 1 \times 10^{-8}$ s.

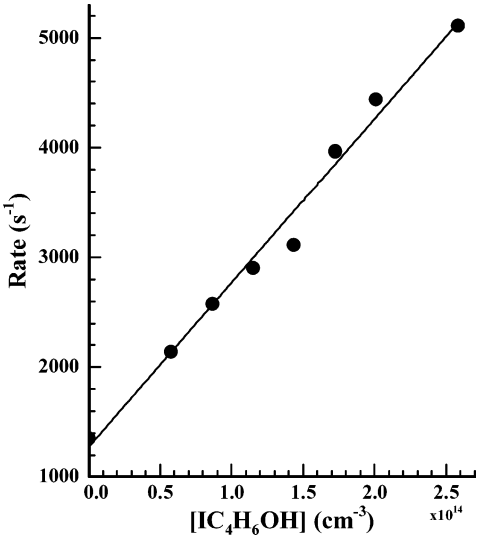

Figure 5. Pseudo-first-order rate constants vs 1-iodo-3-buten-2-ol concentration for the reaction between OD and 1-iodo-3-buten-2-ol.

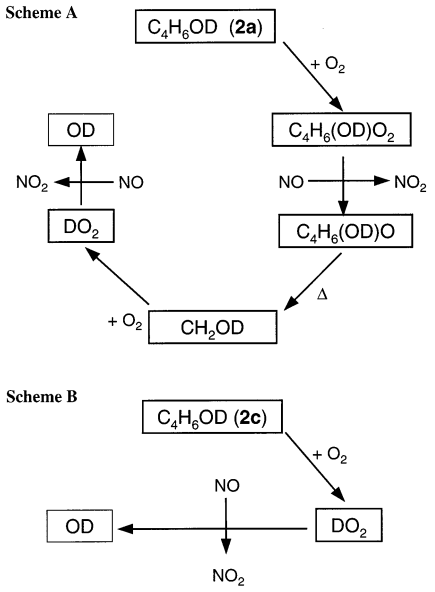

Figure 6. Reaction mechanisms for the subsequent reactivity of the α- and β-hydroxyalkyl radicals in the presence of O_2 and NO. Scheme A is the reaction mechanism for the β-hydroxyalkyl radical, where Scheme B is the reaction mechanism for the α-hydroxyalkyl radical.

Torr at 298 K, we predict that the reactions of both β-hydroxyalkyl radicals and α-hydroxyalkyl radicals with molecular oxygen are important pathways in the atmosphere when considering OH addition to the inner positions of conjugated olefins. Quasi-steady-state fractional populations as a function of condition are provided inTable 2.

C. The Kinetics of OD Formation. The kinetics studies seek to confirm the importance of the β-hydroxyalkyl radical isomerization pathway and to determine the 298 K rate constant for the O_2 reaction with the α-hydroxyalkyl radical. These experiments rely on the measurement of time-dependent OD formation as a function of O_2 and NO concentrations to provide information about the rate constants of intermediate reactions. The technique has been shown to be effective with judicious choice of experimental conditions guided by sensitivity analysis.[14,56]

We observe prompt OD signal following photolysis even in the absence of O_2 and NO. This signal is the result of the small fraction of highly excited hydroxyalkyl radicals (Figure 2) which undergo decomposition to OD and 1,3-butadiene prior to collisional stabilization, and is predicted by the RRKM/ME calculations in section IIIB. In the absence of O_2 and NO, this OD signal exhibits an exponential decay due to reaction with the 1-iodo-3-buten-2-ol precursor. We have determined the rate constant for the reaction of OD with 1-iodo-3-buten-2-ol (nondeuterated) at 298 ± 2 K and 50 Torr total pressure using D_2O_2 photolysis at 248 nm as a source of OD.[57] D_2O_2 was prepared from the hydrogen−deuterium exchange of a D_2O/H_2O_2 solution and detailed information is available elsewhere.[14] Figure 5 shows a typical set of measured pseudo-first-order OD decay rates versus 1-iodo-3-buten-2-ol concentrations. Each OD decay was averaged for up to 100 shots and typically followed over 2 orders of magnitude. We have determined a bimolecular rate constant of $(1.5 \pm 0.1) \times 10^{-11}$ molecule^{-1} cm^3 s^{-1} where the error bars reflect 2σ on the linear fit to the data. Based on the previous studies of the OH/OD reaction with unsaturated hydrocarbons, we believe that the measured rate constant can be considered close to the high-pressure-limit value.

In the presence of O_2 and NO, photolysis of the monodeuterated iodohydrin precursor results in an OD signal that exhibits an initial rise over ~80 μs (Figure 7) followed by a long time decay (inset). We find that the long time decay is not consistent with the reaction with 1-iodo-3-buten-2-ol as the sole OD sink but involves a more complex set of reactions including OD cycling from the precursor analogous to the isoprene system that has been recently studied.[10,11,14] A full investigation of this set of reactions is beyond the scope of the present work. Based on sensitivity analysis (vide infra), we focus our attention on the initial OD formation at short times (<80 μs) where the kinetics are dominated by a limited number of reactions.

The RRKM/ME results, discussed in section IIIB, demonstrate that the cyclic isomerization and collisional deactivation of the nascent β-hydroxyalkyl radicals is "prompt" on the time scale of the subsequent kinetics. As a result, the starting conditions for the kinetics fix the initial concentration of OD and initial concentrations of β-hydroxyalkyl and α-hydroxyalkyl radicals, the later two species being potential sources of OD in the presence of O_2 and NO. The formation of OD from the two hydroxyalkyl radicals occurs by significantly different mechanisms, and this difference permits isolation of the reaction of α-hydroxyalkyl radical with O_2. The production of OD from β-hydroxyalkyl radicals involves several intermediate steps (Figure 6): the addition of O_2,[58] the reaction of the resulting

TABLE 3: Reaction Mechanism and Corresponding Rate Constants (298 K; in molecules^{-1} cm^3 s^{-1} unless the unit is specified) Used for Simulation

	reaction	rate	ref
k_1	α-hydroxyalkyl radical ($CH_2CH(OD)CHCH_2$)	70%	present work
k_2	β-hydroxyalkyl radical (CH_2CHCH_2CHOD)	30%	present work
k_3	$CH_2CHCH_2CHOD + O_2 \rightarrow CH_2CHCH_2CHO + DO_2$	3.3×10^{-11}	present work
k_4	$CH_2CHCH_2CHOD + NO \rightarrow CH_2CHCH_2CH(OD)NO$	2.2×10^{-11}	68, 69, 70, 71
k_5	$CH_2CH(OD)CHCH_2 + NO \rightarrow CH_2CH(OD)(NO)CHCH_2$	2.2×10^{-11}	68, 69, 70, 71
k_6	$CH_2CH(OD)CHCH_2 + O_2 \rightarrow O_2CH_2CH(OD)CHCH_2$	2.3×10^{-12}	14, 68
k_7	$O_2CH_2CH(OD)CHCH_2 + NO \rightarrow OCH_2CH(OD)CHCH_2 + NO_2$	8.5×10^{-12}	11, 13, 14
k_8	$O_2CH_2CH(OD)CHCH_2 + NO \rightarrow ONO_2CH_2CH(OD)CHCH_2$	4.5×10^{-13}	72, 73
k_9	$OCH_2CH(OD)CHCH_2 \rightarrow CH_2O + DOCHCHCH_2$	5.0×10^5 s^{-1}	6
k_{10}	$OCH_2CH(OD)CHCH_2 + NO \rightarrow ONOCH_2CH(OD)CHCH_2$	3.0×10^{-11}	68, 69, 70, 71
k_{11}	$DOCHCHCH_2 + O_2 \rightarrow OCHCHCH_2 + DO_2$	3.0×10^{-11}	27
k_{12}	$DOCHCHCH_2 + NO \rightarrow DOCHCHCH_2NO$	3.0×10^{-11}	68, 69, 70, 71
k_{13}	$DO_2 + NO \rightarrow OD + NO_2$	1.1×10^{-11}	62, 63
k_{14}	$OD + NO \rightarrow DONO$	9.4×10^{-13}	74
k_{15}	$OD + NO_2 \rightarrow DONO_2$	2.2×10^{-12}	74
k_{16}	$OD + IODCH_2CHCHCH_2$	1.5×10^{-11}	present work

peroxy radicals with NO to form alkoxy radicals, decomposition of these radicals, the reaction of the decomposition products with O_2 to yield DO_2, and finally the conversion of DO_2 to OD via reaction with NO. Recent OH/OD cycling experiments on isoprene,[14] for which the β-hydroxyalkyl radicals are the dominant species following OH/OD addition, suggest that, under the conditions employed in the present experiment, the time scale of OD formation from the β-hydroxyalkyl radicals should occur on the order of >200 μs. In contrast, the formation of OD from α-hydroxyalkyl radicals requires only two reaction steps (Figure 6): D abstraction by O_2 followed by conversion of the DO_2 to OD by reaction with NO. Figure 7 shows a typical set of time-dependent OD data using concentrations of 1-iodo-3-buten-2-ol and NO of 6.50×10^{14} and 6.49×10^{14} molecules cm^{-3}, respectively. The OD traces have been offset for clarity. The individual curves represent various concentrations of O_2 ranging from 4.20×10^{14} to 1.69×10^{15} molecules cm^{-3}. The experimental time-dependent OD curves exhibit a rapid increase during the initial 80 μs consistent with a significant yield of α-hydroxyalkyl radicals. Figure 8 shows data obtained by fixing the O_2 concentration at 8.40×10^{14} molecules cm^{-3} and varying the NO concentration between 2.99×10^{14} and 1.30×10^{15} molecules cm^{-3}.

A numerical program, KINTECUS,[59] was used to simulate the kinetics data and the sensitivity analysis was performed using the same software. Initial simulations of the OD curves involved a large set of reactions which included the fate of the radicals arising from OD addition to 1-iodo-3-buten-2-ol and subsequent steps up until OD regeneration. An abridged set of 16 reactions used in the kinetics simulations shown in Figures 7 and 8, and selected based on sensitivity analysis, is given in Table 3 along with the rate constants corresponding to each step. Although the simulations are not sensitive to the *absolute* concentrations of prompt OD, α-hydroxyalkyl radical, and β-hydroxyalkyl radical, the *relative* concentrations of these species are coupled since all three species are related to the short time fate of the nascent β-hydroxyalkyl radicals. The initial concentration of nascent β-hydroxyalkyl radicals is determined by estimating the fraction of 1-iodo-3-buten-2-ol photolyzed at 266 nm.[60] To fit the data, we must include a contribution of "prompt" OD equal to (5 ± 3)% of the nascent β-hydroxyalkyl radical concentration. This yield is qualitatively consistent with our RRKM/ME

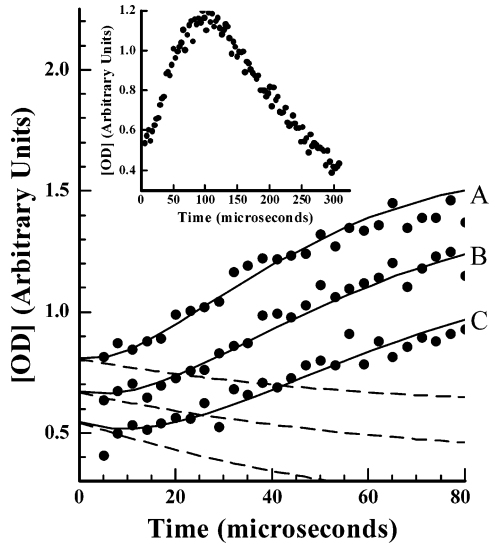

Figure 7. Temporal OD fluorescence intensity at several O_2 concentrations. The curves have been offset for clarity. Symbols represent experimental data and solid lines represent the fits using the reaction mechanism and rate constants in Table 3 with [NO] = 6.49×10^{14} molecules cm^{-3}. The O_2 concentrations were varied: (A) 1.69×10^{15} molecules cm^{-3}; (B) 8.40×10^{14} molecules cm^{-3}; and (C) 4.20×10^{14} molecules cm^{-3}. The dashed lines are simulations assuming only β-hydroxyalkyl radicals are present, i.e., cyclization is negligible. The inset plot shows the long time behavior of OD time profile.

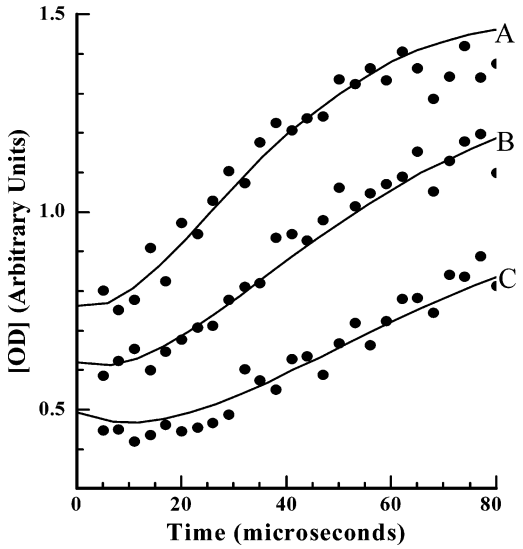

Figure 8. Temporal OD fluorescence intensity at several NO concentrations. Symbols represent experimental data and solid lines represent the fits using the reaction mechanism and rate constants in Table 3 with [O_2] = 8.40×10^{14} molecules cm^{-3}. The NO concentrations were varied: (A) 1.30×10^{15} molecules cm^{-3}; (B) 6.49×10^{14} molecules cm^{-3}; and (C) 2.99×10^{14} molecules cm^{-3}.

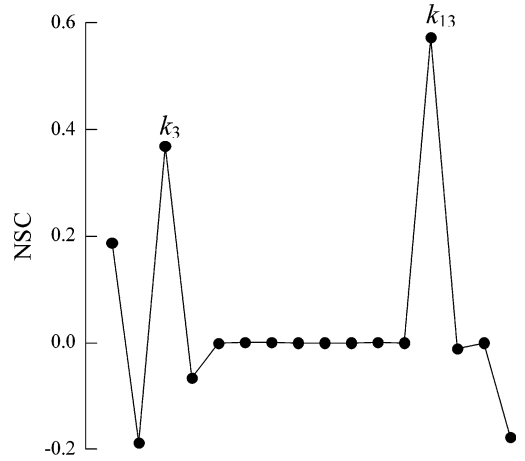

Figure 9. Normalized sensitivity coefficients evaluated at a delay time of 30 μs and with [NO] = 6.49×10^{14} molecules cm^{-3} and [O_2] = 8.40×10^{14} molecules.

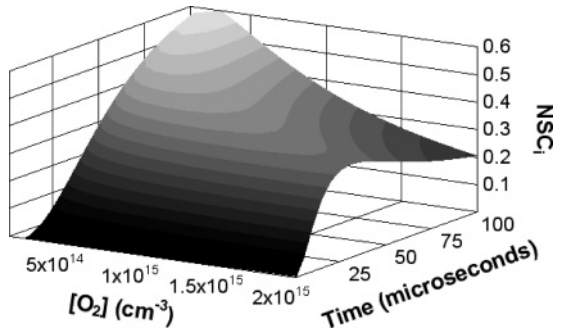

Figure 10. Normalized sensitivity coefficient for the rate constant associated with O_2 reaction with the α-hydroxyalkyl radical.

calculations. The best fits of the simulations to the data are shown as solid lines in Figures 7 and 8. The dashed lines in Figure 7 represent the simulations predicted if the kinetics involved no α-hydroxyalkyl radicals, i.e., the cyclization reaction is negligible. These simulations exhibit an exponential decay of the initial OD, due to the reaction with the precursor, and level off at much longer times due to OD cycling.[10,13,14] Figure 9 shows normalized sensitivity coefficients for all the rate constants in the abridged reaction mechanism evaluated at 30 μs and NO and O_2 concentrations of 6.49×10^{14} and 8.40×10^{14} molecules cm^{-3}, respectively. The figure demonstrates that the OD concentration profiles depend sensitively on few rate constants, in particular, the relative branching between α-hydroxyalkyl and β-hydroxyalkyl radicals (k_1 and k_2),[61] the rate of O_2 reaction with α-hydroxyalkyl radicals (k_3), the rate constant for the reaction between NO and DO_2 (k_{13}), and the rate between OD and 1-iodo-3-buten-2-ol (k_{16}). The rate constant between NO and DO_2 (k_{13}) is well established as $1.1 \pm 0.4 \times 10^{-11}$ cm^3 molecules^{-1} s^{-1},[62,63] and we have determined a rate constant of $1.5 \pm 0.1 \times 10^{-11}$ cm^3 molecules^{-1} s^{-1} for the reaction between OD and the photolytic precursor (k_{16}) in the present work. The simulations are relatively insensitive to the remaining rate constants at short times. Figure 10 shows the normalized sensitivity coefficient for the rate constant associated with O_2 reaction with the α-hydroxyalkyl radical as a function of reaction time and O_2 concentration.

We find that good agreement between the data and the simulations can be achieved using an initial distribution corresponding to (70 ± 20)% α-hydroxyalkyl and (30 ± 20)% β-hydroxyalkyl radicals, which is consistent with the RRKM/ME predictions. Further experimental work as a function of total pressure and bath gas would provide additional constraints on this branching ratio and assess the accuracy of the theoretical calculations. We have determined a value of $(3.3 \pm 1.0) \times 10^{-11}$ cm^3 molecules^{-1} s^{-1} for D-abstraction from the α-hydroxyalkyl radicals by O_2 at 298 ± 2 K.[64] This value is within the range of 1.2×10^{-11} to 3.7×10^{-11} cm^3 molecules^{-1} s^{-1} reported by Miyoshi and co-workers[27] for several α-hydroxyalkyl radicals with O_2. The invariance in this rate constant upon isotopic substitution (i.e., OH from the photolysis of nondeuterated precursor) is consistent with a mechanism that involves O_2 addition followed by HO_2/DO_2 elimination.[65−67] In addition, this observation also serves to limit the possible origin of the early time OH/OD in these experiments.

IV. Conclusions

We have demonstrated a photolytic route to studying isomeric selective kinetics of OH-initiated oxidation of unsaturated hydrocarbons using the UV photolysis of iodohydrins. The present study focuses on the reactivity of the nascent β-hydroxyalkyl radical formed when butadiene undergoes oxidation by hydroxyl radical addition. Velocity map ion imaging permits the direct determination of the internal energy distribution of the nascent radical ensuring that the energy distribution of the radicals can be "tuned" to mimic the kinetics of radicals formed from electrophilic-OH addition. The theoretical predictions modeling isomerization vs collisional relaxation of the β-hydroxyalkyl radicals predict a significant proportion of β-hydroxyalkyl radicals isomerize to the α-hydroxyalkyl radical form before collisional relaxation. Early time OD generation during the kinetics experiments offers conclusive evidence supporting the cyclic isomerization to α-hydroxyalkyl radicals.

Acknowledgment. This work was supported by the National Science Foundation (Grant No. CHE-0204705), the Environmental Protection Agency (Grant No. R03-0132), and by the Robert A. Welch Foundation (Grant A-1402). We gratefully acknowledge computer time and software provided by the Texas A&M University Supercomputing Facility, and the Texas A&M University Laboratory for Molecular Simulation is acknowledged.

References and Notes

(1) Fuentes, J. D.; Lerdau, M.; Atkinson, R.; Baldocchi, D.; Bottenheim, J. W.; Ciccioli, P.; Lamb, B.; Geron, C.; Gu, L.; Guenther, A.; Sharkey, T. D.; Stockwell, W. *Bull. Am. Meteorol. Soc.* **2000**, 1537.
(2) Lei, W.; Zhang, R. *J. Phys. Chem. A* **2001**, *105*, 3808.
(3) McGivern, W. S.; Suh, I. S.; Clinkenbeard, A. D.; Zhang, R.; North, S. W. *J. Phys. Chem. A* **2000**, *104*, 6609.
(4) Stevens, P. S.; Seymour E.; Li, Z. *J. Phys. Chem. A* **2000**, *104*, 5989.
(5) Lei, W.; Zhang, R.; McGivern, W. S.; Derecskei-Kovacs, A.; North, S. W. *J. Phys. Chem. A* **2001**, *105*, 471.
(6) Park, J.; Stephens, J. C.; Zhang, R.; North. S. W. *J. Phys. Chem. A* **2003**, *107*, 6408.
(7) Dibble, T. S. *J. Phys. Chem. A* **2002**, *106*, 6643.
(8) Zhao, J.; Zhang. R.; North, S. W. *Chem. Phys. Lett.* **2003**, *369*, 204.
(9) Zhang, D.; Zhang, R.; Park, J.; North, S. W. *J. Am. Chem. Soc.* **2002**, *124*, 9600.
(10) Campuzano-Jost, P.; Williams, M. B.; D'Ottone, L.; Hynes, A. *J. Phys. Chem. A* **2003**, *109*, 1537.
(11) Stevens, P.; L'Esperance, D.; Chuong, B.; Martin, G. *Int. J. Chem. Kinet.* **1999**, *31*, 637.
(12) Reitz, J. E.; McGivern, W. S.; Church, M. C.; Wilson, M. D.; North, S. W. *Int. J. Chem. Kinet.* **2002**, *34*, 255.
(13) Chuong, B.; Stevens, P. S. *J. Geophys. Res.* **2002**, *107*, 4162.
(14) Park, J.; Jongsma, C. G.; Zhang, R.; North, S. W. *J. Phys. Chem.* **2004**, *108*, 10688.
(15) Zhang, D.; Zhang, R.; Church, C.; North, S. W. *Chem. Phys. Lett. A* **2001**, *343*, 49.

(16) Zalyubovsky, S. J.; Glover, B. G.; Miller, T. A.; Hayes, C.; Merle, J. K.; Hadad, C. M. *J. Phys. Chem. A* **2005**, *109*, 1308.

(17) Francisco-Ma'rques, M.; Alvarez-Idaboy, J. R.; Galano, A.; Vivier-Bunge, A. *Phys. Chem. Chem. Phys.* **2003**, *5*, 1392

(18) Paulson S. E.; Seinfeld, J. H. *J. Geophys. Res.* **1992**, *97*, 20703.

(19) Tuazon, E. C.; Atkinson, R. *Int. J. Chem. Kinet.* **1989**, *21*, 1141.

(20) Jenkin, M. E.; Hayman, G. D. *J. Chem. Soc., Faraday Trans.* **1995**, *91*, 1911.

(21) Busch, G. E.; Wilson, K. R. *J. Chem. Phys.* **1972**, *56*, 3639.

(22) Baldwin, J. E. *J. Chem. Soc., Chem. Commun.* **1976**, *18*, 734.

(23) Park, J.; Jongsma, C. G.; Zhang, R.; North, S. W. *Phys. Chem. Chem. Phys.* **2003**, *5*, 3638.

(24) Carter, W. P. L.; Darnall, K. R.; Graham, R. A.; Winer, A. M.; Pitts, J. N., Jr. *J. Phys. Chem.* **1979**, *83*, 2305.

(25) Ohta, T.; Bandow, H.; Akimoto, H. *Int. J. Chem. Kinet.* **1982**, *14*, 173.

(26) Washida, N. *J. Chem. Phys.* **1981**, *75*, 2715.

(27) Miyoshi, A.; Matsui, H.; Washida, N. *J. Phys. Chem.* **1990**, *94*, 3016.

(28) Barluenga, J.; Marco-Arias, M.; González-Bobes, F.; Ballesteros, A.; González, J. M. *Chem. Eur. J.* **2004**, *10*, 1677.

(29) Masuda, H.; Takase, K.; Nishio, M.; Hasegawa, A.; Nishiyama, Y.; Ishii, Y. *J. Org. Chem.* **1994**, *59*, 5550.

(30) Eppink, A. T. J. B.; Parker, D. H. *Rev. Sci. Instrum.* **1997**, *68*, 3477.

(31) Kim, H.; Park, J.; Niday, T.; North, S. W. *J. Chem. Phys.*, submitted.

(32) Felps, S.; Hochmann, P.; Brint, P.; Mcglynn, S. P. *J. Mol. Spectrosc.* **1976**, *59*, 355.

(33) Dribinski, V.; Ossadtchi, A.; Mandelshtam, V. A.; Reisler, H. *Rev. Sci. Instrum.* **2002**, *73*, 2634.

(34) Zare, R. N. *Mol. Photochem.* **1972**, *4*, 1.

(35) Hess, W. P.; Kohler, S. J.; Haugen, H. K.; Leone, S. R. *J. Chem. Phys.* **1986**, *84*, 2143.

(36) Krajnovich, D.; Butler, L. J.; Lee, Y. T. *J. Chem. Phys.* **1984**, *81*, 3031.

(37) Minton, T. K.; Felder, P.; Brudzynski, R. J.; Lee, Y. T. *J. Chem. Phys.* **1984**, *81*, 1759.

(38) Minton, T. K.; Nathanson, G. M.; Lee, Y. T. *J. Chem. Phys.* **1987**, *86*, 1991.

(39) B3LYP/6-311G** energies reflect a bond dissociation energy of 54.8 kcal/mol; however, a reduction of 1/3 of the spin−orbit splitting (21.2 kcal/mol) was included to correctly reflect the ground-state energy of iodine.

(40) We do not anticipate there will be a substantial change in the energy partitioning upon monodeuteration of the iodohydrin.

(41) Frisch, M. J.; Trucks, G. W.; Schlegel, H. B.; Scuseria, G. E.; Robb, M. A.; Cheeseman, J. R.; Montgomery, J. A., Jr.; Vreven, T.; Kudin, K. N.; Burant, J. C.; Millam, J. M.; Iyengar, S. S.; Tomasi, J.; Barone, V.; Mennucci, B.; Cossi, M.; Scalmani, G.; Rega, N.; Petersson, G. A.; Nakatsuji, H.; Hada, M.; Ehara, M.; Toyota, K.; Fukuda, R.; Hasegawa, J.; Ishida, M.; Nakajima, T.; Honda, Y.; Kitao, O.; Nakai, H.; Klene, M.; Li, X.; Knox, J. E.; Hratchian, H. P.; Cross, J. B.; Bakken, V.; Adamo, C.; Jaramillo, J.; Gomperts, R.; Stratmann, R. E.; Yazyev, O.; Austin, A. J.; Cammi, R.; Pomelli, C.; Ochterski, J. W.; Ayala, P. Y.; Morokuma, K.; Voth, G. A.; Salvador, P.; Dannenberg, J. J.; Zakrzewski, V. G.; Dapprich, S.; Daniels, A. D.; Strain, M. C.; Farkas, O.; Malick, D. K.; Rabuck, A. D.; Raghavachari, K.; Foresman, J. B.; Ortiz, J. V.; Cui, Q.; Baboul, A. G.; Clifford, S.; Cioslowski, J.; Stefanov, B. B.; Liu, G.; Liashenko, A.; Piskorz, P.; Komaromi, I.; Martin, R. L.; Fox, D. J.; Keith, T.; Al-Laham, M. A.; Peng, C. Y.; Nanayakkara, A.; Challacombe, M.; Gill, P. M. W.; Johnson, B.; Chen, W.; Wong, M. W.; Gonzalez, C.; Pople, J. A. *Gaussian 03*, Revision C.02; Gaussian, Inc.: Wallingford, CT, 2004.

(42) Becke, A. D. *J. Chem. Phys.* **1993**, *98*, 5648.

(43) Lee, C.; Yang, W.; Parr, R. G. *Phys. Rev. B* **1988**, *37*, 785.

(44) McLean, A. D.; Chandler, G. S. *J. Chem. Phys.* **1980**, *72*, 5639.

(45) Krishnan, R.; Binkley, J. S.; Seeger, R.; Pople, J. A. *J. Chem. Phys.* **1980**, *72*, 650.

(46) Head-Gordon, M.; Pople, J. A.; Frisch, M. J. *Chem. Phys. Lett.* **1988**, *153*, 503.

(47) Pople, J. A.; Head-Gordon, M.; Raghavachari, K. *J. Chem. Phys.* **1987**, *87*, 5968.

(48) Dunning, T. H. *J. Chem. Phys.* **1989**, *90*, 1007.

(49) Greenwald, E. E.; North, S. W.; Georgievskii, Y.; Klippenstein, S. J. *J. Phys. Chem. A.* **2005**, *109*, 6031.

(50) Stein, S. E.; Ravinovitch, B. S. *J. Chem. Phys.* **1973**, *58*, 2438.

(51) Beyer, T. Swinehart, D. R. *ACM Commun.* **1973**, *16*, 379.

(52) Barker, J. R. *MultiWell Software* Ver. 1.3.1; http://aoss.engin.umich.edu/multiwell/; Ann Arbor, MI, 2002.

(53) Barker, J. R. *Int. J. Chem. Kinet.* **2001**, *33*, 232.

(54) Gilbert, R. G.; Smith, S. C. *Theory of Unimolecular and Recombination Reactions*; Blackwell: Oxford, UK, 1990.

(55) A Boltzmann internal energy distribution for the OH-butadiene adduct was calculated, including vibrational and rotational contributions to the density of states, and then offset by the association energy of hydroxyl radical and butadiene (22.4 kcal/mol), which includes both zero point energy and spin−orbit splitting.

(56) Campuzano-Jost, P.; Williams, M. B.; D'Ottone, L.; Hynes, A. *Geophys. Res. Lett.* **2000**, *27*, 693.

(57) We selected nondeuterated 1-iodo-3-buten-2-ol to avoid interference from prompt OD formation in the monodeuterated isotopomer. No significant isotope effect is anticipated for this reaction.

(58) The reaction of the β-hydroxyalkyl radicals with molecular oxygen is thought to occur exclusively via O_2 addition yielding hydroxy peroxy radicals. The hydrogen abstraction reaction is a relatively minor channel. Recommended rate constants for O_2 addition and hydrogen abstraction are 3×10^{-12} and 8×10^{-15} molecules cm^{-3} s^{-1}, respectively. Atkinson, R.; Baulch, D. L.; Cox, R. A.; Hampson, R. F.; Ker, J. A.; Rossi, M. J.; Troe, J. *J. Phys. Chem. Ref. Data* **1997**, *26*, 521.

(59) Ianni, J. C. *Kintecus Windows* Version 2.80, www.kintecus.com, 2002.

(60) We estimate, based on our laser power and spot size at 266 nm, that the β-hydroxyalkyl concentration is approximately 0.5% the precursor concentration in the laser beam volume.

(61) It should be noted that the absolute values of k_1 and k_2 are not meaningful, only their relative values. The rates are made sufficiently fast to be considered instantaneous on the time scale of the kinetics.

(62) Glaschick-Schimpf, I.; Leiss, A.; Monkhouse, P. B.; Schurath, U.; Becker, K. H.; Fink, E. H. *Eur. Comm., Rep. EUR* **1980**, *EUR 6621*, 122.

(63) Glaschick-Schimpf, I.; Leiss, A.; Monkhouse, P. B.; Schurath, U.; Becker, K. H.; Fink, E. H. *Chem. Phys. Lett.* **1979**, *67*, 318.

(64) We expect there to be no normal kinetic isotope effects associated with this rate constant as is consistent with the reaction between other α-hydroxyalkyl radicals and O_2. The mechanism associated with this step is presumably an association/dissociation reaction. Grother, H.; Riekert, G.; Walter, D.; Just, T. *J. Phys. Chem.* **1988**, *92*, 4028. Evleth, E. M.; Melius, C. F.; Rayez, M. T.; Rayez, J. C.; Forst, W. *J. Phys. Chem.* **1993**, *97*, 5040. Dibble, T. S. *Chem. Phys. Lett.* **2002**, *355*, 193. Hermans, I.; Muller, J.; Nguyen, T. L.; Jacobs, P. A.; Peeters, J. *J. Phys. Chem. A* **2005**, *109*, 4303.

(65) Grotheer, H.; Riekert, G.; Walter, D.; Just, T. *J. Phys. Chem.* **1988**, *92*, 4028.

(66) Dibble, T. S. *Chem. Phys. Lett.* **2002**, *355*, 193.

(67) Hermans, I.; Muller, J.; Nguyen, T. L.; Jacobs, P. A.; Peeters, J. *J. Phys. Chem. A* **2005**, *109*, 4303.

(68) Atkinson, R. *J. Phys. Chem. Ref. Data* **1997**, *26*, 215.

(69) Lotz, Ch.; Zellner, R. *Phys. Chem. Chem. Phys.* **2001**, *3*, 215.

(70) Deng, W.; Wang, C.; Katz, D. R.; Gawinski, G. R.; Davis, A. J.; Dibble, T. S. *Chem. Phys. Lett.* **2000**, *330*, 541.

(71) Blitz, M.; Pilling, M. J.; Robertson, S. H.; Seakins, P. W. *Phys. Chem. Chem. Phys.* **1999**, *1*, 73.

(72) Chen, X.; Hulbert, D.; Shepson, P. B. *J. Geophys. Res.* **1998**, *103*, 25563.

(73) Sprengnether, M.; Demerjian, K. L.; Donahue, N. M.; Anderson, J. G. *J. Geophys. Res.* **2002**, *107*, 4268.

(74) Calculated using k_0 and k_{inf} values given in DeMore, W. B.; Sander, S. P.; Golden, D. M.; Hampson, R. F.; Kurylo, M. J.; Howard, C. J.; Ravishankara, A. R.; Kolb, C. E.; Molina, M. J. *Chemical Kinetics and Photochemical Data for Use in Stratospheric Modeling*, JPL Publ. 02-25; Jet propulsion Lab: Pasadena, CA, 2003.